An experimental study on dynamic pore wettability

Chemical Engineering Science 104 (2013) 988–997

Contents lists available at ScienceDirect

Chemical Engineering Science

journal homepage: www.elsevier.com/locate/ces

An experimental study on dynamic pore wettability

Xingxun Li [a], Xianfeng Fan [a,*], Alexandros Askounis [a], Kejian Wu [b], Khellil Sefiane [a], Vasileios Koutsos [a]

[a] Institute for Materials and Processes, School of Engineering, The University of Edinburgh, King's Buildings, Mayfield Road, Edinburgh EH9 3JL, United Kingdom
[b] Chevron ETC, San Ramon, CA 94583, USA

HIGHLIGHTS

- We develop a technique to experimentally measure dynamic pore contact angle.
- Dynamic pore contact angle increases monotonically with the contact-line velocity.
- Surface tension and viscosity affect the dynamic pore contact angle significantly.
- A new empirical correlation developed can predict dynamic wetting in a small pore.
- The dynamic contact angle results are correlated with the Crispation number (Cr).

GRAPHICAL ABSTRACT

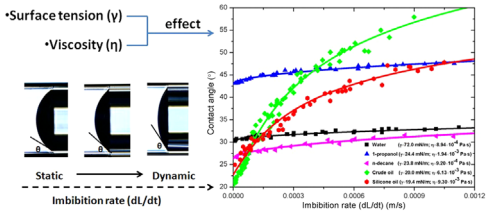

ARTICLE INFO

Article history:
Received 30 August 2013
Received in revised form
9 October 2013
Accepted 15 October 2013
Available online 29 October 2013

Keywords:
Dynamic wetting
Pore wettability
Imbibition dynamics
Surface tension
Viscosity

ABSTRACT

Dynamic pore wettability is important for understanding fluid behavior and adsorption in porous media for enhanced oil recovery, groundwater movements, nanofluidics and nanolubrication. Although dynamic wetting of different liquids has been extensively studied on various plane substrates, dynamic wettability in small pores has not been systematically investigated. In this paper, we measured dynamic contact angles in single glass capillaries with a size range from 100 to 250 μm, in order to investigate the relationship between dynamic contact angle and spontaneous imbibition of various liquids, the effects of surface tension and viscosity of liquids on dynamic contact angle, and the dependence of contact angle on contact-line velocity in a pore. The liquids used are silicone oils with various viscosities, deionized water, 1-propanol, n-decane, crude oil, propanol-water mixtures with various surface tensions. The results indicate that the dynamic contact angle of liquids in a pore increases monotonically with the contact-line velocity at low capillary numbers, and this increase becomes more significant when more viscous liquids or liquids with lower surface tensions are used. A new empirical correlation based on the obtained experimental data has been proposed to describe dynamic pore wettability in a low capillary number range ($1.0\times10^{-7}<\mathrm{Ca}<1.8\times10^{-5}$). Finally, we show that all our results can be summarized by a master curve relating the contact angle variation at a specific velocity with the Crispation number (Cr) signifying the importance of the interfacial deformation of liquid in a pore.

1. Introduction

Dynamic wetting is a feature of the motion of liquid–liquid or liquid–gas interfaces in porous media, and is of significant importance

* Corresponding author. Tel.: +44 131 6505678, fax: +44 1316506551.
E-mail address: x.fan@ed.ac.uk (X. Fan).

0009-2509/$ - see front matter © 2013 Elsevier Ltd. All rights reserved.
http://dx.doi.org/10.1016/j.ces.2013.10.026

in ceramic, coating, printing, detergency, groundwater movements, soil science and oil recovery (Cazabat, 1992; de Gennes, 1985; Dussan, 1979; Elyousfi et al., 1998; Ishimi et al., 1998; Teletzke et al., 1987, 1988), nanofluidics and nanolubrication (Martic et al., 2005). Dynamic wettability is characterized by dynamic contact angle (Latva-Kokko and Rothman, 2005) and is mainly measured through the spreading of liquids onto flat solid surfaces. For instance, Bayer and Megaridis (2006) measured dynamic contact angles during the spontaneous spreading and recoiling of water droplets on flat surfaces with various wetting conditions. Keller et al. (2007) used the Wihelmy plate technique to measure the dynamic contact angles of petroleum hydrocarbons at various advancing velocities. Previous research on flat surfaces has indicated that dynamic contact angle depends on the speed of solid–liquid–gas contact line, and varies with drop volume, viscosity, surfactant concentration, flow geometry, fluid composition and solid surface properties (Carré and Eustache, 1997, 2000; Dezellus et al., 2002; Min et al., 2011; Roques-Carmes et al., 2010; Wang et al., 2007).

Dynamic wetting of liquids can be described by several theories such as the hydrodynamic theories proposed by Cox (1986), Voinov (1976), Dussan (1976) and the molecular-kinetic theory introduced by Blake and Haynes (1969). Combined models have also been attempted to describe contact line motion of spreading liquids by Petrov and Petrov (1992). A number of empirical correlations (Jiang et al., 1979; Bracke et al., 1989; Seebergh and Berg, 1992) and semi-empirical correlations (Rillaerts and Joos, 1980; Ishimi et al., 1986; Ström et al., 1990) have been proposed to predict the dynamic contact angle (θ_d) by using the static contact angle (θ_s) and the capillary number (Ca). The capillary number (Ca) is defined as the ratio of viscous forces to interfacial forces. For instance, Jiang et al. (1979) presented an empirical correlation to describe the dependence of dynamic contact angle on capillary number (Ca) and static contact angle (θ_s) based on Hoffman's data through a study of non-polar liquids spreading. Bracke et al. (1989) gave a similar empirical correlation by drawing polymer strips into liquid. Because Ca and θ_s can be easy to measure, the correlations from Jiang et al. (1979) and Bracke et al. (1989) can be applied to most of three-phase dynamic wetting phenomena when capillary number is less than 0.01. Seebergh and Berg (1992) examined the dynamic contact angle at a low capillary number regime via force measurements by using a dynamic microtensiometer. The correlations proposed by Seebergh and Berg (1992) is a function of contact-line velocity, and have the same functional form as the correlations from Jiang et al. (1979) and Bracke et al. (1989) at low capillary numbers, but with different constants.

In most of dynamic contact angle studies, the Lucas–Washburn equation is often used to calculate the contact angle in a pore using measured capillary imbibition distance and imbibition time (Chibowski and Hoysz, 1997; Martic et al., 2002; Siebold et al., 2000; Xue et al., 2006), but the contact angle calculated from Lucas–Washburn equation is static. To describe the imbibition dynamics, Joos et al. (1990) used velocity-dependent contact angle (θ_v) which was derived from an empirical expression to replace the static contact angle (θ_s) in the classic Lucas–Washburn equation. Martic et al. (2002) modified the classic Lucas–Washburn equation by using Blake's molecular-kinetic theory. Succi group used the molecular-kinetic model to describe the micro-capillary imbibition dynamics considering the friction effect on the three-phase moving line, and the modeling results matched the experimental data well (Girardo et al., 2012). Stukan et al. (2010) investigated the effect of roughness on the spontaneous imbibition of liquid in nanopores by coarse grain molecular dynamics simulation and used the Blake's molecular-kinetic theory to describe the effect of dynamic contact angle on liquid imbibition. Because of lack of experimental techniques to measure the dynamic contact angle in a small pore, most of the experimental or theoretical works on dynamic wettability were based on the data measured from a flat solid plate, strip or cylindrical rod rather than in pores (Seebergh and Berg, 1992). It is commonly assumed that the contact angle on a flat surface can represent the wetting condition in a pore. This might be true in some cases but deserves to be assessed (Gomez et al., 2000). So, it is crucial and necessary to directly measure dynamic contact angles in a pore to advance the understanding of dynamic multiphase interfaces advancing through the porous medium.

In this paper, dynamic wetting behavior in a pore was studied in a low capillary number regime from 10^{-7} to 10^{-2}. Since an ensemble of single pores with simplified geometries is accepted as representation of pore system (Friedman, 1999), the main objectives of this work were therefore to directly measure the dynamic contact angles for various liquids imbibed into single glass capillaries in order to describe the dependence of dynamic contact angle on imbibition rate. The results showed the effects of surface tension and viscosity of liquids on the dynamic contact angle in a pore, which were well explained by the Crispation number (Cr). A new empirical correlation was developed to describe the dynamic wetting in a pore in a low capillary number regime.

2. Theories and equations

2.1. Hydrodynamic and molecular-kinetic theories

The dynamic wetting can be described by the hydrodynamics models proposed by Cox (1986), Voinov (1976), Dussan (1976) and Blake's molecular-kinetics theory (Blake and Haynes, 1969). The hydrodynamic theory and molecular-kinetic model consider dissipation effects during imbibitions due to the viscous friction in the bulk and to the solid characteristics at the moving contact line, respectively (Girardo et al., 2012). According to the hydrodynamic model, the spreading process is dominated by viscous dissipation. Viscous friction in the bulk is the controlling mechanism for the motion of the contact line. Cox–Voinov equation is a simple description of the contact line motion and the driving force (deviation of the contact angle from equilibrium) (Cox, 1986; Voinov, 1976):

$$v = \frac{\gamma}{9\eta \ln\left(\frac{\ell}{a}\right)}(\theta_d^3 - \theta_s^3) \tag{1}$$

where θ_d is the dynamic contact angle, θ_s is the static (equilibrium) contact angle, η is the liquid viscosity and γ is the liquid–vapor interfacial tension. ℓ/a is the ratio of macroscopic to microscopic length scales. Brochard-Wyart and de Gennes (1992) derived an equivalent expression by considering the spreading as an irreversible process and calculating the energy dissipation per length of unit line. The velocity of the contact line is then given by:

$$v = \frac{\theta\gamma}{6\eta \ln\left(\frac{\ell}{a}\right)}(\cos\,\theta_s - \cos\,\theta_d) \tag{2}$$

Blake developed a molecular-kinetic theory of three-phase moving line based on Eyring's activated-rate theory with an adsorption/desorption model (Blake and Haynes, 1969). The imbibition rate (penetration velocity) is given by:

$$v = \frac{dL}{dt} = 2K_0\lambda\,\sin\,h\left[\frac{\gamma(\cos\,\theta_s - \cos\,\theta_d)}{2nk_BT}\right] \tag{3}$$

Where K_0 is the frequency of molecular displacement, n denotes adsorption sites per unit area ($n^{-1}=\lambda^2$), λ is the average length of each molecular displacement, T is the temperature and k_B denotes Boltzmann constant ($k_B = 1.381\times10^{-23}\,\mathrm{J\,K^{-1}}$). The term of $\gamma(\cos\,\theta_s - \cos\,\theta_d)$ can be regarded as the nonequilibrated surface tension force to drive the motion of the wetting line.

The effects of viscosity and interfacial tension can be basically reflected in molecular-kinetic theory (Blake and Haynes, 1969) and hydrodynamic theories (Cox, 1986; de Gennes, 1985; Dussan, 1976; Voinov, 1976); any increase in bulk viscosity or decrease in interfacial tension leads to slower contact line velocity (Eqs. (1–3)), $v \sim \gamma(\cos\theta_s - \cos\theta_d)/\eta$. In other words, the contact-line velocity is proportional to the ratio between the driving force (per unit triple line length) ($F \sim \gamma(\cos\theta_s - \cos\theta_d)$), and viscosity η (Blake, 2006; Bonn et al., 2009).

2.2. Empirical correlations for dynamic wetting

The dynamic wetting could be expressed by empirical correlations proposed by Jiang et al. (1979), Bracke et al. (1989), Seebergh and Berg (1992). All these three empirical correlations express the dynamic contact angle as a function of the capillary number (Ca) and the static contact angle (θ_s).

$$\theta_d = f\ (\mathrm{Ca},\ \theta_s) \tag{4}$$

where Ca is the capillary number defined as the ratio of viscous forces to interfacial forces ($\mathrm{Ca} = v\,\eta/\gamma$).

All these three empirical correlations can be unified to a "universal function" (Seebergh and Berg, 1992) which only applies for $\mathrm{Ca} < 0.01$, as

$$H = \frac{\cos\theta_s - \cos\theta_d}{\cos\theta_s + 1} = A\mathrm{Ca}^B \tag{5}$$

$$\log_{10} H = B\ \log_{10}\mathrm{Ca} + \log_{10} A \tag{6}$$

where H is the dimensionless function for dynamic contact angle, A and B are correlation constants. Although the correlations can follow the linear relationship between $\log_{10} H$ and $\log_{10}\mathrm{Ca}$, different constants (A, B) were required to fit the data. (Table 1)

3. Methods and materials

3.1. Manufacturing and cleaning of glass capillary tubes

The glass capillaries with inner diameters of 100–250 μm were used in the measurements. They are made from clean glass tubes with diameters of 1 mm (Bilbate, CAP-100-10). The glass tubes were washed by using hot concentrated sodium hydroxide (Fisher Scientific, 10 M concentrate), concentrated nitric acid (Fisher Scientific, 10 M concentrate), acetone (Fisher Scientific, A/0600/15), and then rinsed thoroughly with deionized water (Fisher and Lark, 1979; Xue et al., 2006). The glass tubes were then heated up to 550 °C on flame to remove any residue of organic contamination and were kept in ash-proof enclosure (Fisher and Lark, 1979). The single capillaries with various sizes were obtained by melting the middle section of dry and clean glass tubes on butane flame (Butane Battery, D2-BS 0167) and drawing the tube to a long distance in order to make sure that the size of capillary is uniform. The size difference between the two ends of the capillary measured under microscope is $\pm 1.5\% \times$ capillary diameter.

Table 1
Empirical correlations for dynamic wetting in literatures.

Author	Empirical correlation	Correlation constants in Eqs. (5) and (6)	
		A	B
Jiang et al. (1979)	$\frac{\cos\theta_s - \cos\theta_d}{\cos\theta_s + 1} = 4.96\ \mathrm{Ca}^{0.702}$	4.96	0.702
Bracke et al. (1989)	$\frac{\cos\theta_s - \cos\theta_d}{\cos\theta_s + 1} = 2\ \mathrm{Ca}^{0.5}$	2.0	0.5
Seebergh and Berg (1992)	$\frac{\cos\theta_s - \cos\theta_d}{\cos\theta_s + 1} = 4.47\ \mathrm{Ca}^{0.42}$	4.47	0.42

3.2. Atomic force microscopy (AFM) imaging of capillary interiors

Due to the sensitive dependence of dynamic wetting on surface cleanness and roughness, the glass capillary pore inner surfaces were analyzed using an AFM (Bruker AXS, Santa Barbara, CA). A Bruker Multimode/Nanoscope III AFM equipped with an E-scanner (x–y scan range about 10 μm) used to scan the inner walls of capillaries, under both contact and tapping modes. For contact mode CSC21 Ultrasharp cantilevers (Mikromasch, Wetzlar, Germany) were used, with nominal spring constant of 2.0 N/m and resonance frequency of 105 kHz, respectively, and a nominal tip radius of less than 10 nm, as specified by the manufacturer. For tapping mode (tip in intermediate contact with the surface) Bruker RTESP cantilevers were used, with nominal spring constants of 40 N/m and resonance frequencies of 300 kHz, respectively, and a nominal tip radius of about 8 nm, as specified by the manufacturer. Cantilevers were oscillated vertically at 5% below their natural resonant frequency and moved in a raster fashion within the specified region of interest. All scans were performed in air at room temperature.

To image the inner walls of the capillaries, short sections of glass capillaries were placed in the middle of two double-side tapes and crushed (Danisman et al., 2008). The top tape was then removed to ensure the exposed surfaces of the crushed capillaries on the bottom tape facing upwards and representing the inner walls of the capillaries. These exposed capillary interiors were then identified and selected for AFM imaging using a Nikon SMZ745T stereoscope (Nikon, Tokyo, Japan) situated above the cantilever. Each sample was imaged at several different areas. The roughness and height profiles of inner wall surfaces of capillaries were further analyzed by the Scanning Probe Image Processor (SPIP, Image Metrology, Hϕsholm, Denmark). Both modes yielded similar results and we present here typical images, height profiles and roughness measurements for each capillary.

Fig. 1 indicates that the inner surfaces of glass capillaries were homogeneous with no indication of organic contaminants (we note that the phase imaging in tapping mode gave no contrast). The inner surface roughness of the capillaries used ranges from 1.6 nm to 3.0 nm, which are almost the same, in terms of contact angle measurements. This small range of inner surface roughness does not significantly affect the dynamic contact angle as shown in Fig. 3 in Section 4.1.

3.3. Dynamic contact angle measurements

The advancing dynamic contact angle measurement apparatus used in this study is shown in Fig. 2. The liquid meniscus was imaged by an optical microscope (Olympus, BHW) with a 10X objective (M PLAN 10X (025)) equipped with a digital camera (AM7023, Dino-Eye) (Fig. 2 (a)). Since the quality of meniscus image of a small volume of liquid in a capillary highly depends on the measurement method and light source, a LED light source was placed under the glass capillary. The light travels from the liquid end up to the meniscus in a dark background to overcome the degree of image distortion when a cylindrical capillary is used and therefore facilitate the measurements (Cheong et al., 2011). The outmost boundary of liquid–gas interface was well lighted and focused to produce the clear two-phase interfacial line (Danisman et al., 2008; Kohonen, 2006). This method is similar to the principle used in measuring micron air-bubble size (Fan et al., 2004), micron ice crystal size in aqueous solution (Fan et al., 2003) and the size of a plant cell or a microcapsule in water under a microscope (Rosiński et al., 2002).

During the measurement, the cleaned single glass capillary was first fixed onto a glass slide support and focused by the

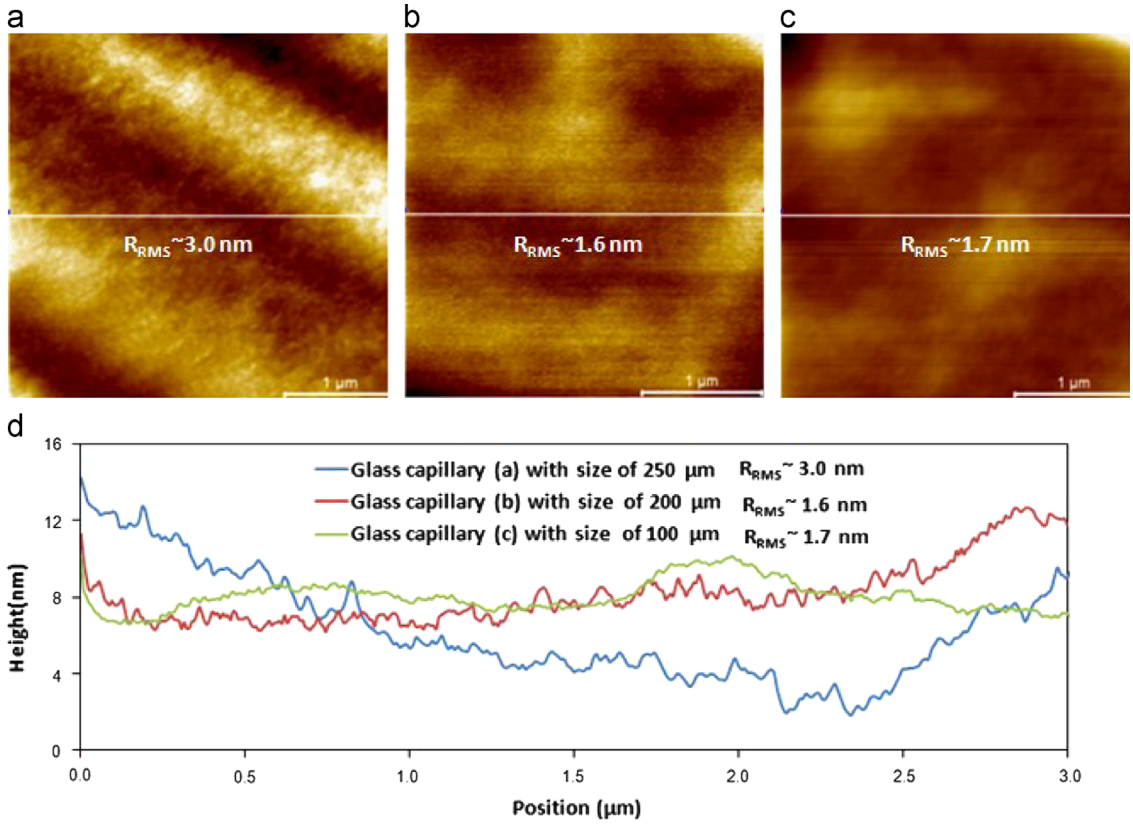

Fig. 1. AFM images of the inner wall surfaces of capillaries with different sizes. (a) 250 μm, surface roughness: 3.0 nm; (b) 200 μm, surface roughness: 1.6 nm; (c) 100 μm, surface roughness: 1.7 nm. Image size = 3 × 3 μm^2, *z*-scale = 16 nm. (d) Average height profiles corresponding to selected paths (from left to right) in each image of the inner wall surfaces of capillaries with sizes of (a) 250 μm, (b) 200 μm and (c) 100 μm.

microscope (Fig. 2). The experiment was started by dropping a small amount of liquid (0.5 μL) onto one end of the capillary by a microfluidics syringe (Hamilton, 701ASN 10 μL) at ambient conditions. The liquid was then imbibed into the capillary by its own capillary force. The dynamic advancing liquid–gas menisci were recorded by camera tracking to obtain the dynamic contact angles at different liquid–gas interface velocities (Fig. 2(b)). The imbibition rates ($v = dL/dt$) were obtained by analysis of each image which was extracted from the recorded video with video editing software (Adobe Premiere Pro 2.0). Each imbibition distance interval (dL) was measured within the imbibition time interval of 0.3 s ($dt = 0.3$ s). The static contact angle was achieved when the imbibition and any dynamic movement of liquid were completely stopped and the equilibrium status of liquid in the capillary was reached. The effect of evaporation of liquid on contact angle measurement at ambient condition could be negligible in this study due to the limited micro-size pores and the short measurement time. Each measurement was repeated up to five times to confirm the reliability of experimental data.

In order to obtain the contact angle of liquid in a pore, we analyzed the microscopic images by using the method recently proposed by Cheong et al. (2011). Cheong et al. (2011) developed a method of measuring the contact angle of small volumes, by only using the capillary radius (r) and meniscus height (h) (Fig. 2 (a)) of the capillary meniscus (Eq. (7)).

$$\theta = \tan^{-1}\left(\frac{r^2 - h^2}{2rh}\right) \tag{7}$$

where θ is the contact angle in a pore, r is the radius of capillary and h the height of capillary meniscus.

3.4. Materials

Considering the effect of the physical properties of liquids on dynamic contact angles in a pore, six types of liquids were chosen to investigate the dynamic contact angle in a single glass capillary at ambient conditions (20 °C, 1 atm). The six liquids are deionized water, 1-propanol (Acros Organics, analytic grade, 99+% pure), 1-propanol aqueous solutions with various concentrations (5 wt%, 10 wt%, 20 wt%, 40 wt%, 60 wt%, 80 wt% and 90 wt%), n-decane (Acros Organics, analytic grade, 99+% pure), crude oil (MAPLLC Petroleum Crude Oil), and silicone oils with various viscosities (9.30×10^{-3} Pa · s, 4.80×10^{-2} Pa · s, 9.60×10^{-2} Pa · s, 4.85×10^{-1} Pa · s and 9.70×10^{-1} Pa s) (Sigma-Aldrich, Dow Corning Corporation 200® fluid). The surface tensions of these liquids were determined by pendant drop experiments (First Ten Angstroms).

Since the dynamic contact angle is correlated to the capillary number ($Ca = v\,\eta/\gamma$) and the static contact angle (θ_s) (Eq. (4)), the surface tension and viscosity of liquid are therefore the crucial parameters in determining the dynamic contact angle in a pore (Hoffman, 1975; Jiang et al., 1979; Meiron et al., 2004). In this study, experiments were therefore mainly designed to investigate the effects of liquid viscosity and surface tension on dynamic wetting. The effect of surface tension on dynamic contact angle was achieved by using 1-propanol aqueous solutions with various concentrations, water and 1-propanol. The water, 1-propanol and 1-propanol aqueous solutions have similar viscosities, but their surface tensions dramatically vary from 72.0 mN/m (water) to 24.4 mN/m (1-propanol) as shown in Table 2. The silicone oils with various viscosities of 9.30×10^{-3} Pa s, 4.80×10^{-2} Pa s, 9.60×10^{-2} Pa s, 4.85×10^{-1} Pa s and $9.70 \times$

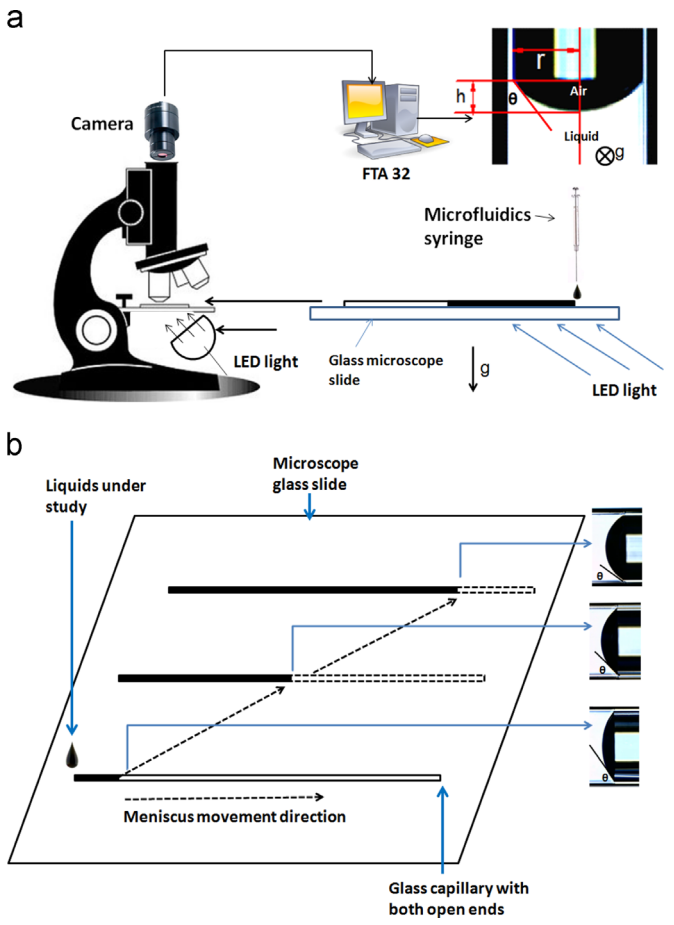

Fig. 2. Experimental setup for the study of dynamic contact angles in a capillary. (a) Microscopic imaging of contact angle of liquids in a pore (the vector $\overline{g}$ shows the direction of gravity); (b) Dynamic contact angles (meniscus movements) under a microscope equipped with a camera.

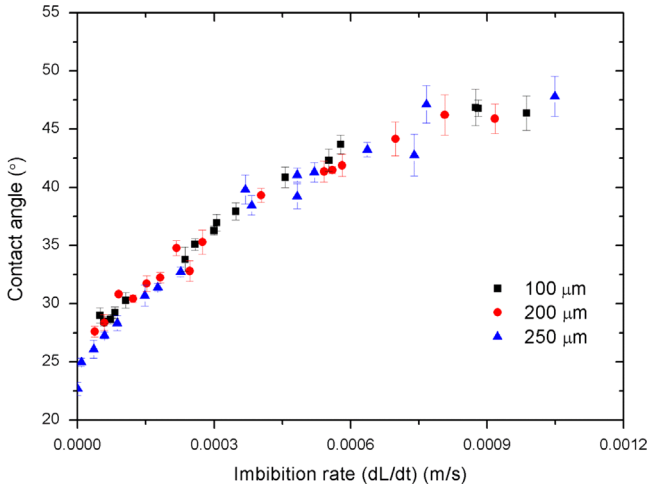

Fig. 3. Dynamic contact angle of silicone oil (η=9.30 × 10^{-3} Pa s) in glass capillaries with different pore sizes of 100 μm, 200 μm and 250 μm.

10^{-1} Pa s were used to study the impact of liquid viscosity on dynamic pore wetting.

Table 2
The physical properties of liquids investigated.

Liquids	Density[a] (kg/m^3)	Surface tension[b] (mN/m)	Viscosity[a] (Pa s)	Thermal diffusivity[a,c] (m^2/s)
DI water	998.2	72.0	8.94×10^{-4}	1.39×10^{-7}
1-propanol	803.4	23.7	1.94×10^{-3}	7.90×10^{-8}
5 wt% 1-propanol	987.9	46.2	1.10×10^{-3}	1.36×10^{-7}
10 wt% 1-propanol	976.1	37.3	1.34×10^{-3}	1.33×10^{-7}
20 wt% 1-propanol	953.3	30.3	1.84×10^{-3}	
40 wt% 1-propanol	910.8	27.8	2.44×10^{-3}	
60 wt% 1-propanol	872.0	27.2	2.67×10^{-3}	
80 wt% 1-propanol	836.3	26.3	2.41×10^{-3}	
90 wt% 1-propanol	819.5	25.0	2.17×10^{-3}	
n-decane	730.0	23.8	9.20×10^{-4}	8.16×10^{-8}
Crude oil	659–818	20.0	6.14×10^{-3}	
Silicone oil (10cst)	930.0	19.4	9.30×10^{-3}	9.86×10^{-8}
Silicone oil (50cst)	960.0	20.8	4.80×10^{-2}	9.56×10^{-8}
Silicone oil (100cst)	960.0	20.9	9.60×10^{-2}	9.56×10^{-8}
Silicone oil (500cst)	970.0	21.2	4.85×10^{-1}	9.46×10^{-8}
Silicone oil (1000cst)	970.0	21.2	9.70×10^{-1}	9.46×10^{-8}

[a] The fundamental physical properties of the liquids (density, viscosity, thermal conductivity and heat capacity) were taken from NIST Chemistry WebBook (2005) and the product property specifications by manufacturer. The viscosities of 1-propanol aqueous solutions were obtained from the literature data (Fong-Meng et al., 2007).

[b] The surface tensions of liquids were determined by pendant drop experiments (First Ten Angstroms).

[c] Thermal diffusivity is defined as the thermal conductivity (α) divided by density (ρ) and specific heat capacity (C_p) of liquid, $\alpha = k/(\rho C_P)$. The thermal diffusivities of 5 wt% and 10 wt% 1-propanol aqueous solutions were estimated by the weighted average method based on the thermal diffusivities and the mass fractions of water and 1-propanol, $\alpha_{1-propanol\ aqueous\ solution} = \alpha_{water} x_{water} + \alpha_{1-propanol} x_{1-propanol}$ where α_{water} and $\alpha_{1-propanol}$ are thermal diffusivities of water and 1-propanol, respectively and x_{water} and $x_{1-propanol}$ are mass fractions of water and 1-propanol, respectively.

4. Results and discussion

4.1. Dynamic contact angles in glass capillaries

Fig. 3 shows the dynamic contact angles of silicone oil with a viscosity of 9.30 × 10^{-3} Pa s in glass capillaries with a pore size range from 100 to 250 μm and a roughness range from 1.6 to 3.0 nm measured by AFM (Fig. 1). It can be clearly seen that the dynamic contact angle monotonically increases with imbibition rate. At the liquid–gas interface velocity of zero, the contact angle of silicone oil is around 22.7° and corresponds to the static contact angle. The dynamic contact angle increases roughly by 28° when the velocity increases from 0 to 0.0012 m/s. The effect of pore size on the dynamic contact angle is not significant within the pore size range from 100 to 250 μm at low capillary numbers. Our results clearly show that the dynamic contact angle depends on imbibition rate, but do not indicate a pore size dependence because of the narrow size range used. All our data for this range of pore sizes (100–250 μm) used in this study are similar as Fig. 3 indicates.

Fig. 4 shows the dynamic contact angles of water, 1-propanol, n-decane, crude oil and silicone oil in glass capillaries when the imbibition rate was from 0 to 0.0012 m/s. It can be clearly seen that the dynamic contact angles of silicone oil and crude oil are highly velocity-dependent, while the dynamic contact angle profiles of water, 1-propanol and n-decane are less velocity-dependent. When the imbibition rate increased from 0 to 0.0012 m/s, the dynamic contact angles of water, 1-propanol and n-decane varied only by 3.0–5.2°. By contrast, the dependences of dynamic contact angles of crude oil and silicone oil on imbibition rate are much more remarkable due to their larger viscosities. The dynamic contact angles of crude oil increased from 20° to 60°, and

the dynamic contact angle of silicone oil ($\eta=9.30\times10^{-3}$ Pa s) increased from 22° to 50°. The physical and chemical properties of these five liquids are very different. The dependence of dynamic contact angle on contact-line velocity might be influenced by the combination of effects from surface tension and viscosity of liquid. Thus, these two significant factors will be investigated separately in the following section to find out the effects of surface tension and viscosity of liquids on dynamic contact angles of liquids in a pore, respectively.

4.2. *Effects of surface tension and viscosity of liquids on dynamic contact angle in a pore.*

Fig. 5 shows the effect of surface tension of liquids on the dynamic contact angle in a pore. To measure the effect of surface tension, we have to minimize the effect of liquid viscosity. In this study, water, 1-propanol and its aqueous solutions were used. Water, 1-propanol and 1-propanol aqueous solutions have a very low viscosity from 8.94×10^{-4} to 1.94×10^{-3} Pa·s, but their surface tensions vary significantly from 24.4 to 72.0 mN/m. The results indicate that the variations of dynamic contact angles of these four liquids with imbibition rate followed very similar trends (Fig. 5(a)), but different magnitudes (Fig. 5(b)). The difference between the cosine of the static contact angle and the dynamic contact angle at imbibition rate of 0.0012 m/s ($\cos\theta_s-\cos\theta_d$) increased linearly with the reciprocal of surface tension ($1/\gamma$). 1-propanol has the lowest surface tension (24.4 mN/m), while its dynamic contact angle varies with the imbibition rate most significantly by 5.2°. 10 wt% 1-propanol solution and 5 wt% 1-propanol solution have higher surface tensions (37.3 mN/m and 46.2 mN/m, respectively), but their dynamic contact angles vary only by 4.8° and 4.2°, respectively. The smallest difference between static and dynamic contact angles came from water with a variation only by 3.0°. Thus, it can be concluded that the dependence of dynamic wetting on contact-line velocity is affected by surface tension of liquid and much more significantly for the liquid with lower surface tension.

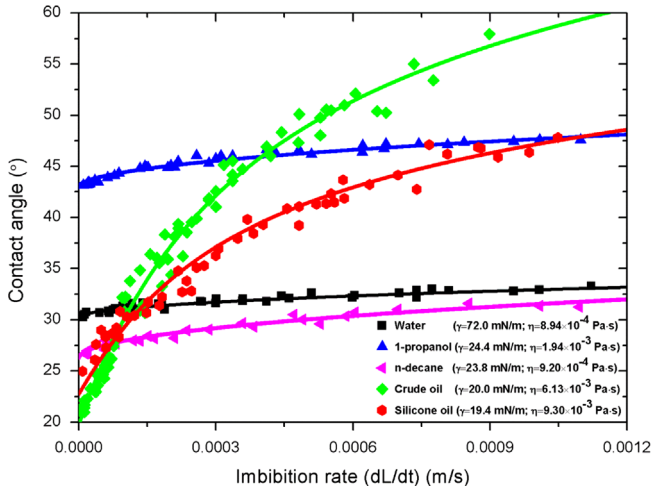

Fig. 4. Dynamic contact angles of DI water, 1-propanol, n-decane, crude oil and silicone oil ($\eta=9.30\times10^{-3}$ Pa s) in a pore.

To investigate the effect of viscosity of liquid on the dynamic pore wettability, silicone oils were used. The silicone oils have a very similar surface tension, but their viscosity significantly varies from 9.30×10^{-3} Pa s to 9.70×10^{-1} Pa s. Fig. 6 shows the effect of liquid viscosity on the dynamic contact angle in a pore. The results indicate that viscosity significantly influences the dynamic contact angle, but not the static contact angle (Fig. 6(a)). When the viscosity increased from 9.30×10^{-3} Pa s to 9.70×10^{-1} Pa s, the static contact angles of silicone oils stay around 23°, while the dynamic contact angles of more viscous silicone oils are always higher than those from less viscous silicone oils. Fig. 6(b) shows that the difference between the cosine of the static contact angle and dynamic contact angle at imbibition rate of 0.0012 m/s increases in approximately linear fashion with the logarithm of viscosity.

Thus, it can be concluded that the dynamic contact angle varies with imbibition rate more significantly for the liquid with lower surface tension or higher viscosity. The magnitude of the dynamic contact angle (θ_d) is a result of an interplay between two main forces: capillary forces (surface-tension-driven force), which tend to reduce θ_d in the case of an advancing wetting fluid, and viscous forces, which tend to increase θ_d under the same conditions (Friedman, 1999). At the low speed of liquid flow in porous materials, it is expected that the dependence of the contact angle on the moving interface velocity will be more significant for the liquids of higher viscosity and lower liquid–gas surface tension, for example, the dynamic contact angle depends on the velocity more remarkably for NAPLs than water (Friedman, 1999).

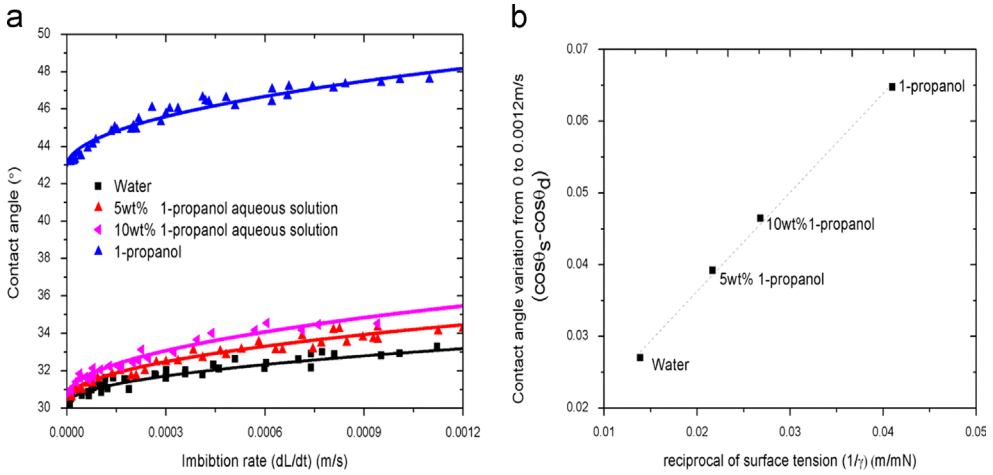

Fig. 5. (a) Dynamic contact angle and (b) the contact angle variation ($\cos\theta_s-\cos\theta_d$) from 0 to 0.0012 m/s of water ($\gamma=72.0$ mN/m; $\eta=8.94\times10^{-4}$ Pa s), 1-propanol ($\gamma=24.4$ mN/m; $\eta=1.94\times10^{-3}$ Pa s), 5 wt% 1-propanol aqueous solution ($\gamma=46.2$ mN/m; $\eta=1.10\times10^{-3}$ Pa s) and 10 wt% 1-propanol aqueous solution ($\gamma=37.3$ mN/m; $\eta=1.34\times10^{-3}$ Pa s) in pores with sizes of 100–250 μm.

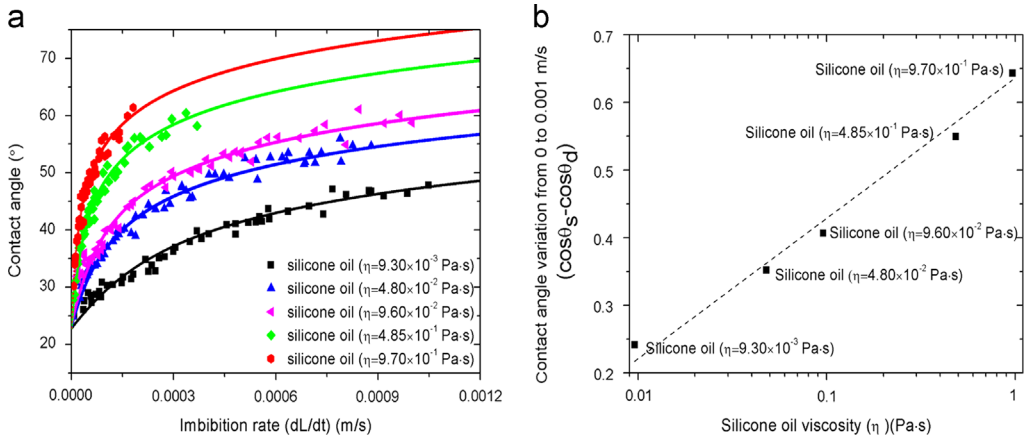

Fig. 6. (a) Dynamic contact angle and (b) contact angle variation ($\cos\theta_s - \cos\theta_d$) from 0 to 0.0012 m/s of silicone oils with different viscosities of 9.30×10^{-3} Pa s, 4.80×10^{-2} Pa s, 9.60×10^{-2} Pa s, 4.85×10^{-1} Pa · s and 9.70×10^{-1} Pa s and similar surface tensions of 19.4 mN/m, 20.8 mN/m, 20.9 mN/m, 21.2 mN/m and 21.2 mN/m, respectively, in pores with sizes of 100 to 250 μm. The scale in the *x*-axis (the viscosity of silicone oil) of (b) is logarithmic with base 10.

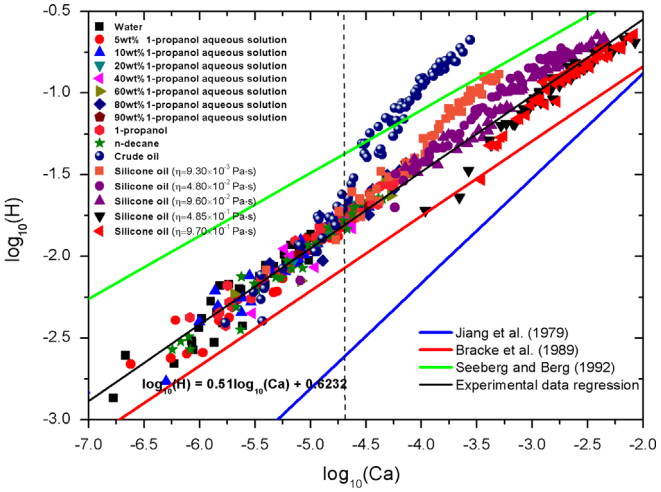

Fig. 7. Comparison of empirical correlations (Table 1) with the experimental data in a low capillary number (Ca) range.

4.3. *A new empirical correlation for dynamic contact angle in a pore at a low capillary number regime*

Several empirical correlations have been developed to predict the dynamic contact angle (Jiang et al., 1979; Bracke et al., 1989; Seebergh and Berg, 1992). The correlations proposed by Jiang et al. (1979) and Bracke et al. (1989) can describe dynamic wetting behavior well for capillary numbers above 10^{-3} in a relatively high capillary number regime. Seebergh and Berg (1992) extended the dynamic wetting measurements into the low capillary number region ($10^{-3} < \mathrm{Ca} < 10^{-7}$). They found that the correlations given by Jiang et al. (1979) and Bracke et al. (1989) can not fit their data at lower capillary numbers. Thus, Seebergh and Berg (1992) developed an empirical correlation to describe wetting behavior at low capillary numbers by considering the stick-slip effect. To the authors' best knowledge, these correlations have not been applied to the dynamic contact angle in a micro-size pore. Fig. 7 presents the comparison of our measurements with the results calculated from the existing empirical correlations, which are plotted using $\log_{10}(\mathrm{H})$ against $\log_{10}(\mathrm{Ca})$ according to Eq. (6). It can be seen that our experimental results differ from the predictions from Jiang et al. (1979), Bracke et al. (1989), and Seebergh and Berg (1992) empirical correlations. The results indicate that our measured $\log_{10}(H)$ for all of the liquids are very close and increase linearly with $\log_{10}(\mathrm{Ca})$ when the liquid capillary number ($\log_{10}(\mathrm{Ca})$) is less than -4.75. When the liquid capillary number ($\log_{10}(\mathrm{Ca})$) is greater than -4.75, the measured $\log_{10}(H)$ varies with liquids used. The crude oil gave the highest $\log_{10}(H)$. This most significant difference in dynamic contact angle from crude oil might be due to the dewetting behavior caused by the effect of surfactants in the crude oil on the invading interface (Afsar-Siddiqui et al., 2003a, 2003b, 2004; Craster and Matar, 2007). The results calculated from the correlations proposed by Jiang et al. (1979) and Bracke et al. (1989) are much smaller than our experimental data. The dynamic contact angles of liquids in a pore calculated using Seebergh and Berg (1992) correlation are different from and larger than our experimental results, even though the similar capillary regime was investigated in Seebergh and Berg (1992) correlation and this study. The Seebergh and Berg (1992) correlation was developed to describe the dynamic wetting of those systems in which the stick-slip effects produced a large degree of scatter. The stick-slip effects were caused by rough surfaces. Since our inner wall surfaces were relatively smooth, the stick-slip effect is not significant.

Because of the very good linear relationship between $\log_{10}(H)$ and $\log_{10}(\mathrm{Ca})$ in the region with a capillary number $\log_{10}(\mathrm{Ca})$ range from -7.0 to -4.75, a linear least-square fit of experimental data yields (Eq. (8)). This adopts the same format of the empirical correlation (Eqs. (5) and (6)) in which the $\log_{10}(H)$ increases linearly with $\log_{10}(\mathrm{Ca})$ (Fig. 7),

$$H = 4.2\ \mathrm{Ca}^{0.51} \tag{8}$$

Eq. (8) is a regression of dynamic contact angles in a pore based on our experimental data. It lies between Bracke et al. (1989) and Seebergh and Berg (1992) correlations, but the constants A and B in Eq. (6) differ from those given by Jiang et al. (1979) and Bracke et al. (1989) and Seebergh and Berg (1992). This newly developed empirical correlation can describe the dynamic pore wetting for the liquids with a capillary number ($\log_{10}(\mathrm{Ca})$) lower than -4.75 in a low capillary number regime ($1.0\times10^{-7} < \mathrm{Ca} < 1.8\times10^{-5}$).

4.4. *Description of the interface deformation by crispation number (Cr)*

In what follows we attempt to summarize all experimental data in order to deduce a trend which describes the change in contact angle as a function of the physical properties of liquids used. We adopt a dimensionless number i.e. the Crispation number, Cr, which is commonly used in convection and interfacial stability studies to describe deformability of the interface. It is the ratio between dynamic viscosity, η and surface tension, γ considering thermal diffusivity, α and length scale (pore radius), ℓ constant

$Cr = \eta\alpha/\gamma\ell$. Although the problem at hand is somewhat different from interfacial instabilities, nonetheless the physics behind the Crispation number should be useful. Indeed we would like to examine the degree of deformation of the interface (represented by the change in angle, $\Delta\theta$) of the meniscus inside the pore under various constraints, i.e. imbibition velocities and for a variety of liquids. Unlike the capillary number which includes an operating condition i.e. velocity, the Crispation number consists entirely of the physical properties of the working liquid.

The change in contact angle for a given imbibition velocity is a good indication of the deformation of the interface. Therefore the change in contact angle, θ_v, at a given velocity compared to the static case at zero velocity, θ_s, is plotted as a function of Crispation number. In doing so, we make use of all the experimental data obtained in this study. On semi-log plot the data show a linear increase in contact angle variation with Crispation number (Fig. 8). The trend is consistent for all investigated imbibition velocities and over many orders of magnitude of Crispation number, which is more than satisfactory. It is worth noting that at very low Crispation numbers there might be a slight variation in dependence of deformation on Crispation number. Exploring various possible regimes in different ranges of Crispation numbers is however beyond the scope of this study.

The relationship between the change in contact angle and Crispation number can be described as follows, $\Delta\theta \sim \log Cr$. The slope of the linear increase in contact angle with Crispation number is dictated by the imbibition velocity, v. This representation is very useful and can have some practical implications, as it gives an idea on the degree of change in wettability as a function of physical properties of working liquids, with the imbibition velocity as a parameter.

Based on the above representation of the change in contact angle as a function of the Crispation number, one can examine some extreme cases. Let us first examine the case of varying surface tension of the liquid and how it affects the interface deformation in the pore. When surface tension tends to infinity, the Crispation number tends to infinitely small values which results in a zero change in contact angle. This is equivalent to a rigid almost hard interface. The other extreme case is when surface tension tends to zero, then the Crispation number tends to infinity and the change in the contact angle in a pore tends to 90°. This situation can describe well the flow of a supercritical fluid in a pore, since the interface disappears at critical point. A similar discussion can be performed for the dynamic viscosity of working liquids. However for the sake of brevity, we limit our discussion to surface tension. Overall, the experimental data presented in this study allowed deducing some consistent trends which are undoubtedly of some significance to a wide range of applications. Future work could examine a wider range of physical properties of liquids as well as the effect of the nature of the pore material which has not been examined in the present investigation.

5. Conclusions

The present study mainly focuses on the direct measurements of the dynamic contact angles of various liquids in a pore and investigates the effects of surface tension and viscosity of liquids on the dynamic pore wettability. A new empirical correlation was developed to predict the dynamic contact angles liquids in a small pore at a low capillary regime. The results indicate that:

(1) The dynamic contact angle of liquid in a pore depends on and increases monotonically with the contact-line velocity at low capillary numbers.

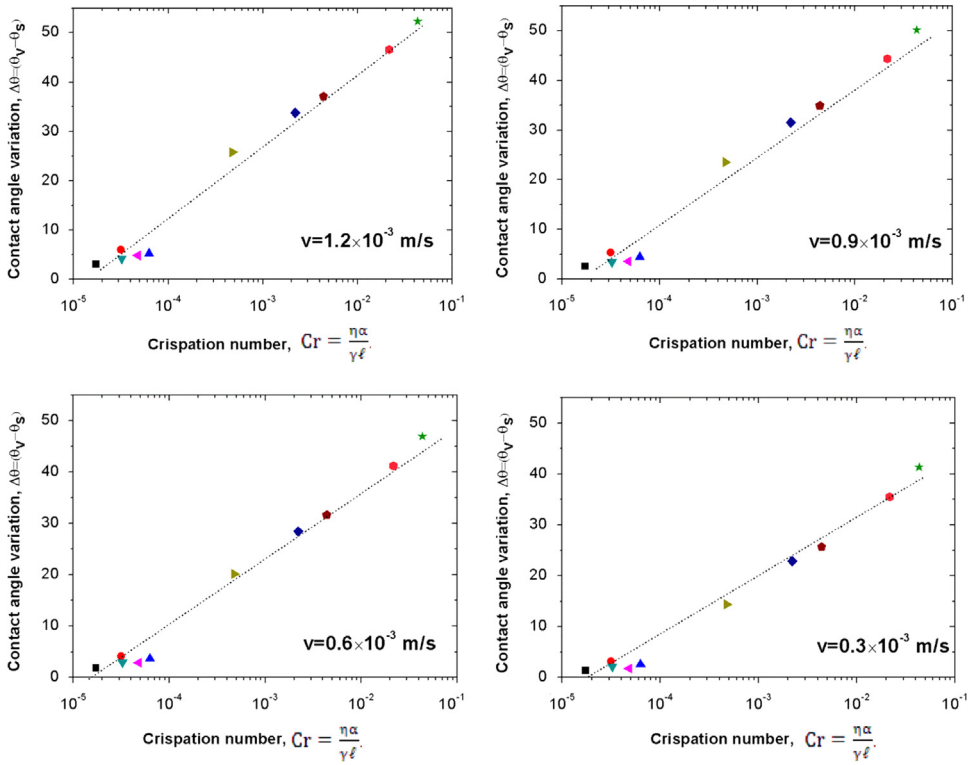

Fig. 8. Contact angle change as a function of Crispation number for various imbibition velocities (as a parameter) in the pore with a size of 200 μm. Water (■), n-decane (●), 1-propanol (▲), 5 wt% 1-propanol aqueous solution (▼), 10 wt% 1-propanol aqueous solution (◀), silicone oil (9.30×10^{-3} Pa s) (▶), silicone oil (9.60×10^{-2} Pa s) (◆), silicone oil (4.80×10^{-2} Pa s) (⬟), silicone oil (4.85×10^{-1} Pa s) (⬢), silicone oil (9.70×10^{-1} Pa s) (★). The dotted lines are a cue for the eye. θ_v are the dynamic contact angles (θ_d) at the imbibition rates of 1.2×10^{-3} m/s, 0.9×10^{-3} m/s, 0.6×10^{-3} m/s and 0.3×10^{-3} m/s, respectively.

(2) Surface tension and viscosity of liquids affect the dynamic contact angle in a pore significantly. A low liquid–gas surface tension tends to favor the variation of dynamic contact angle with imbibition rate. The liquid with higher viscosity has a more significant effect on the dynamic pore wettability alteration.
(3) A new empirical correlation (Eq. (8)) developed based on our experimental data can predict the dynamic contact angles for liquids in a small pore at a low capillary regime ($1.0\times10^{-7}<\mathrm{Ca}<1.8\times10^{-5}$).
(4) All experimental data were finally used to deduce a trend which describes the change in contact angle as a function of a dimensionless number (Crispation number, Cr, which involves the main physical properties of the liquids), in order to explain from the physical point of view (interfacial deformation) the effects of the combination of surface tension and viscosity of liquids on the dynamic pore wettability.

Acknowledgments

This work is supported by the Carnegie Scholarship, UK, University of Edinburgh Research Scholarship, the Research Grant from the UK Royal Society (e-gap) and the Royal Academy of Engineering for research exchange scheme. We also would like to thank the technique support from Mr. Gardiner Hill, the Director of Technology at BP, Dr. Stephen J. Cawley at BP, and Dr. Jinhai Yang and Heron from the Heriot-Watt University, and thank Mr. Stephen Mitchell in School of Biological Sciences of The University of Edinburgh for SEM measurements.

Appendix A. Supplementary material

Supplementary data associated with this article can be found in the online version at http://dx.doi.org/10.1016/j.ces.2013.10.026.

References

Afsar-Siddiqui, A.B., Luckham, P.F., Matar, O.K., 2003a. Unstable spreading of aqueous anionic surfactant solutions on liquid films. Part 1 sparingly soluble surfactant. Langmuir 19, 696–702.
Afsar-Siddiqui, A.B., Luckham, P.F., Matar, O.K., 2003b. Unstable spreading of aqueous anionic surfactant solutions on liquid films. 2. Highly soluble surfactant. Langmuir 19, 703–708.
Afsar-Siddiqui, A.B., Luckham, P.F., Matar, O.K., 2004. Dewetting behavior of aqueous cationic surfactant solutions on liquid films. Langmuir 20, 7575–7582.
Bayer, I.S., Megaridis, C.M., 2006. Contact angle dynamics in droplets impacting on flat surfaces with different wetting characteristics. J. Fluid Mech. 558, 415–449.
Blake, T.D., 2006. The physics of moving wetting lines. J. Colloid Interface Sci. 299, 1–13.
Blake, T.D., Haynes, J.M., 1969. Kinetics of liquid/liquid displacement. J. Colloid Interface Sci. 30, 421–423.
Bracke, M., De Voeght, F., Joos, P., 1989. The kinetics of wetting: the dynamic contact angle. Prog. Colloid Polym. Sci. 79, 142–149.
Bonn, D., Eggers, J., Indekeu, J., Meunier, J., Rolley, E., 2009. Wetting and spreading. Rev. Mod. Phys. 81, 739–805.
Brochard-Wyart, F., de Gennes, P.G., 1992. Dynamics of partial wetting. Adv. Colloid Interface Sci. 39, 1–11.
Carré, A., Eustache, F., 1997. Dynamique d'étalement d'un liquide rhéofluidifiant. Comptes Rendus de l'Académie des Sci. Ser. IIB Mech. Phys.Chem. Astron. 325, 709–718.
Carré, A., Eustache, F., 2000. Spreading kinetics of shear-thinning fluids in wetting and dewetting modes. Langmuir 16, 2936–2941.
Cazabat, A.M., 1992. Wetting from macroscopic to microscopic scale. Adv. Colloid Interface Sci. 42, 65–87.
Cheong, B.H.-P., Ng, T.W., Yu, Y., Liew, O.W., 2011. Using the meniscus in a capillary for small volume contact angle measurement in biochemical applications. Langmuir 27, 11925–11929.
Chibowski, E., Hoysz, L., 1997. On the use of Washburn's equation for contact angle determination. J. Adhes. Sci. Technol. 11, 1289–1301.
Cox, R.G., 1986. The dynamics of the spreading of liquids on a solid surface. Part 1 viscous flow. J. Fluid Mech. 168, 169–194.
Craster, R.V., Matar, O.K., 2007. On autophobing in surfactant-driven thin films. Langmuir 23, 2588–2601.
Danisman, M.F., Calkins, J.A., Sazio, P.J.A., Allara, D.L., Badding, J.V., 2008. Organosilane self-assembled monolayer growth from supercritical carbon dioxide in microstructured optical fiber capillary arrays. Langmuir 24, 3636–3644.
de Gennes, P.G., 1985. Wetting statics and dynamics. Rev. Mod. Phys. 57, 827–863.
Dezellus, O., Hodaj, F., Eustathopoulos, N., 2002. Chemical reaction-limited spreading: the triple line velocity versus contact angle relation. Acta Mater. 50, 4741–4753.
Dussan, V ,E.B., 1979. On the spreading of liquids on solid surfaces: static and dynamic contact lines. Annu. Rev. Fluid Mech. 11, 371–400.
Dussan, V.E.B., 1976. On the difference between a bounding surface and a material surface. J. Fluid Mech. 75, 609–623.
Elyousfi, A.B.A., Chesters, A.K., Cazabat, A.M., Villette, S., 1998. Approximate solution for the spreading of a droplet on a smooth solid surface. J. Colloid Interface Sci. 207, 30–40.
Fan, X., Ten, P., Clarke, C., Bramley, A., Zhang, Z., 2003. Direct measurement of the adhesive force between ice particles by micromanipulation. Powder Technol. 131, 105–110.
Fan, X., Zhang, Z., Li, G., Rowson, N.A., 2004. Attachment of solid particles to air bubbles in surfactant-free aqueous solutions. Chem. Eng. Sci. 59, 2639–2645.
Fisher, L.R., Lark, P.D., 1979. An experimental study of the washburn equation for liquid flow in very fine capillaries. J. Colloid Interface Sci. 69, 486–492.
Fong-Meng, P., Chye-Eng, S., Tjoon-Tow, T., Ibrahim, M.H., 2007. Densities and viscosities of aqueous solutions of 1-propanol and 2-propanol at temperatures from 293.15 K to 333.15 K. J. Mol. Liq. 136, 71–78.
Friedman, S.P., 1999. Dynamic contact angle explanation of flow rate-dependent saturation-pressure relationships during transient liquid flow in unsaturated porous media. J. Adhes. Sci. Technol. 13, 1495–1518.
Girardo, S., Palpacelli, S., De Maio, A., Cingolani, R., Succi, S., Pisignano, D., 2012. Interplay between shape and roughness in early-stage microcapillary imbibition. Langmuir 28, 2596–2603.
Gomez, F., Denoyel, R., Rouquerol, J., 2000. Determining the contact angle of a nonwetting liquid in pores by liquid intrusion calorimetry. Langmuir 16, 4374–4379.
Hoffman, R.L., 1975. A study of the advancing interface. I. Interface shape in liquid-gas systems. J. Colloid Interface Sci. 50, 228–235.
Ishimi, K., Hikita, H., Esmail, M.N., 1986. Dynamic contact angles on moving plates. AIChE J. 32, 486–492.
Ishimi, K., Mohri, J., Mukouyama, H., Ishikawa, H., 1998. Dynamic wetting and advancing contact angles in horizontal capillary tubes. J. Chem. Eng. Jpn. 31, 914–921.
Jiang, T.S., Oh, S.G., Slattery, J.C., 1979. Correlation for dynamic contact angle. J. Colloid Interface Sci. 69, 74–77.
Joos, P., van Remoortere, P., Bracke, M., 1990. The kinetics of wetting in a capillary. J. Colloid Interface Sci. 136, 189–197.
Keller, A.A., Broje, V., Setty, K., 2007. Effect of advancing velocity and fluid viscosity on the dynamic contact angle of petroleum hydrocarbons. J. Pet. Sci. Technol. 58, 201–206.
Kohonen, M.M., 2006. Engineered wettability in tree capillaries. Langmuir 22, 3148–3153.
Latva-Kokko, M., Rothman, D.H., 2005. Static contact angle in lattice Boltzmann models of immiscible fluids. Phys. Rev. E 72, 046701.
Martic, G., Blake, T.D., De Coninck, J., 2005. Dynamics of imbibition into a pore with a heterogeneous surface. Langmuir 21, 11201–11207.
Martic, G., Gentner, F., Seveno, D., Coulon, D., De Coninck, J., Blake, T.D., 2002. A molecular dynamics simulation of capillary imbibition. Langmuir 18, 7971–7976.
Meiron, T.S., Marmur, A., Saguy, I.S., 2004. Contact angle measurement on rough surfaces. J. Colloid Interface Sci. 274, 637–644.
Min, Q., Duan, Y.-Y., Wang, X.-D., Liang, Z.-P., Si, C., 2011. Does macroscopic flow geometry influence wetting dynamic? J. Colloid Interface Sci. 362, 221–227.
NIST, 2005. NIST Chemistry WebBook, NIST Standard Reference Database Number 69. National Institute of Standards and Technology.
Petrov, P.G., Petrov, J.G., 1992. A combined molecular-hydrodynamic approach to wetting kinetics. Langmuir 8, 1762–1767.
Rillaerts, E., Joos, P., 1980. The Dynamic contact angle. Chem. Eng. Sci. 35, 883–887.
Roques-Carmes, T., Mathieu, V., Gigante, A., 2010. Experimental contribution to the understanding of the dynamics of spreading of Newtonian fluids: Effect of volume, viscosity and surfactant. J. Colloid Interface Sci. 344, 180–197.
Rosiñski, S., Grigorescu, G., Lewiñska, D., Ritzén, L.G., Viernstein, H., Teunou, E., Poncelet, D., Zhang, Z., Fan, X., Serp, D., Marison, I., Hunkeler, D., 2002. Characterization of microcapsules: recommended methods based on round-robin testing. J. Microencapsul. 19, 641–659.
Seebergh, J.E., Berg, J.C., 1992. Dynamic wetting in the low capillary number regime. Chem. Eng. Sci. 47, 4455–4464.
Siebold, A., Nardin, M., Schultz, J., Walliser, A., Oppliger, M., 2000. Effect of dynamic contact angle on capillary rise phenomena. Colloids Surf. A: Physicochem. Eng. Asp. 161, 81–87.
Ström, G., Fredriksson, M., Stenius, P., Radoev, B., 1990. Kinetics of steady-state wetting. J. Colloid Interface Sci. 134, 107–116.
Stukan, M.R., Ligneul, P., Crawshaw, J.P., Boek, E.S., 2010. Spontaneous imbibition in nanopores of different roughness and wettability. Langmuir 26, 13342–13352.

Teletzke, G.F., Davis, H.T., Scriven, L.E., 1987. How liquids spread on solids. Chem. Eng. Comm. 55, 41–82.
Teletzke, G.F., Davis, H.T., Scriven, L.E., 1988. Wetting hydrodynamics. Rev. Phys. Appl. 23, 989–1007.
Voinov, O.V., 1976. Fluid Dynamics (English Translation of Izvestiya Akademii Nauk SSSR, Mekhanika Zhidkosti i Gaza). Hydrodyn. Wetting 11, 714–721.
Wang, X.D., Lee, D.J., Peng, X.F., Lai, J.Y., 2007. Spreading dynamics and dynamic contact angle of non-newtonian fluids. Langmuir 23, 8042–8047.
Xue, H.T., Fang, Z.N., Yang, Y., Huang, J.P., Zhou, L.W., 2006. Contact angle determined by spontaneous dynamic capillary rises with hydrostatic effects: Experiment and theory. Chem. Phy. Lett., 432; , pp. 326–330.